Systems analysis of metabolism in platelet concentrates during storage in platelet additive solution

Freyr Jóhannsson[1,2], Steinn Guðmundsson[1], Giuseppe Paglia[3], Sveinn Guðmundsson[4], Bernhard Palsson[1], Ólafur E. Sigurjónsson[4, 5] and Óttar Rolfsson[1,2]*.

[1]Center for Systems Biology, University of Iceland, Sturlugata 8, Reykjavik, Iceland.
[2]Medical Department, University of Iceland, Sturlugata 8, Reykjavik, Iceland.
[3]Center for Biomedicine, European Academy of Bolzano/Bozen, Via Galvani 31, Bolzano, Italy
[4]The Blood Bank, Landspitali-University Hospital, Snorrabraut 60, Reykjavik, Iceland.
[5]School of Science and Engineering, Reykjavik University, Menntavegur 1, Reykjavik Iceland.
*Corresponding Author

Correspondence: Óttar Rolfsson, Center for Systems Biology, University of Iceland, Sturlugata 8, Reykjavik, Iceland. Telephone: +354 5255854. E-mail: ottarr@hi.is

ABSTRACT

Platelets deteriorate over time when stored within blood banks through a biological process known as platelet storage lesion (PSL). Here we describe the refinement of biochemical network of platelet metabolism iAT-PLT-636 and its application to describe and investigate changes in metabolism during platelet storage. Changes to extracellular acetate and citrate were measured in buffy coat and apheresis platelet units over 10 days of storage in the platelet additive solution T-Sol. Metabolic network analysis of these data was performed alongside our prior metabolomics data to describe the metabolism of fresh (days 1-3), intermediate (days 4-6), and expired (days 7-10) platelets. Changes to metabolism was studied by comparing metabolic model flux predictions of iAT-PLT-636 between stages and between collection methods. Extracellular acetate and glucose contribute most to central carbon metabolism in platelets. The anticoagulant citrate is metabolized in apheresis stored platelets and is converted to aconitate and, to a lesser degree, malate. The consumption of nutrients changes during storage and reflects altered platelet activation profiles following their collection. Irrespective of collection method, a slowdown in oxidative phosphorylation takes place, consistent with mitochondrial dysfunction during PSL. Finally, the main contributors to intracellular ammonium and NADPH are highlighted. Future optimization of flux through these pathways provides opportunities to address intracellular pH changes and reactive oxygen species which are both of importance to PSL. The metabolic models provide descriptions of platelet metabolism at steady state and represent a platform for future platelet metabolic research.

ABBREVIATIONS

platelets (PLTs), platelet storage lesion (PSL), platelet additive solution (PAS), genome scale metabolic network (GEM), platelet concentrate (PC), apheresis derived platelets concentrate, buffy coat derived platelet concentrate, flux balance analysis (FBA), pentose phosphate pathway (PPP), tricarboxylic acid TCA, citrate phosphate dextrose (CPD), principal component analysis (PCA), aldose reductase (AR), mass distribution vector (MDV).

INTRODUCTION

Platelets (PLTs) are blood cells that perform a vital role in wound hemostasis by clogging damaged blood vessels (1) and they also play a critical part in inflammation processes (2). Some blood disorders, cancers, and cancer treatments can lead to abnormally low platelet counts. This is frequently corrected by carrying out blood transfusion of platelet concentrates which are collected and stored at blood banks.

The investigation of platelets within a blood bank allows the understanding of platelet biology to be advanced in a rigorously defined and clinically relevant setting. When platelets are stored over time they sustain loss of function and change in morphology, a condition referred to as platelet storage lesions (PSLs) which mirrors cellular changes that occur during platelet activation and apoptosis (3-5). The storage lesion results from a complex interplay of platelet metabolism and platelet physiology during storage (3) and is known to increase the risk of post-transfusion complications (6). Studies of platelets under storage conditions have been performed since the late 1950s. They have shown that the shelf-life of platelets can be extended by i) using plastic containers that are permeable to oxygen and CO_2 (7); ii) inclusion of sodium chloride in storage solutions (8); iii) pH regulation (9); iv) inclusion of acetate as a buffering agent and a fuel for platelets (10); v) inclusion of citrate as an anticoagulant (10); and vi) keeping glucose consumption and lactate production low (11). Based on these findings, several platelet storage media (termed platelet additive solutions, PAS) have been developed during the last decades and subsequently adopted in the blood bank setting in order to improve platelet quality and storage time.

Blood banking guidelines in the USA dictate that platelets collected via the apheresis method can be stored for up to 5 days. In Europe, platelets collected via the buffy coat method can be stored for up to 7 days. The two main factors limiting the platelet shelf life to such a short time period are the risk of pathogen infection and PSL (4). Prolonging the storage time could lead to significant cost savings for blood banks around the world (12) and by slowing down the PSL, the likelihood of adverse clinical outcomes could be reduced as prolonged storage is inversely correlated with enhanced survival in vivo (13). In order to improve upon the state of the art, a detailed biochemical understanding of PLT metabolism during storage is required.

Genome scale metabolic models (GEMs) integrate sequence, biochemical, and enzymatic data in a structured manner which enables quantitative prediction of phenotypic behavior (14). GEMs are increasingly being used to study human metabolism (reviewed in (15, 16)). A platelet reconstruction termed iAT-PLT-636 (17) has been constructed that forms a basis for data driven platelet metabolic network modelling and analysis (18). The iAT-PLT-636 reconstruction of platelet metabolism is a manually curated cell-scale biochemical network based on 33 proteomic studies and over 350 peer reviewed articles (17). We recently published comprehensive data sets describing platelet metabolism under storage conditions within a controlled blood bank environment (19, 20). The data includes concentration values of multiple intracellular and extracellular metabolites at eight different time points as well as several blood quality control parameters and activation markers, for platelets collected under both apheresis (AP-PC) and buffy coat (BC-PC) conditions and stored in PAS.

Here we describe the advancement of these studies in order to comprehensively describe platelet metabolism during storage in a blood banking environment. We addressed gaps in our previous metabolomics study by measuring acetate and citrate consumption in platelets over time, performed ^{13}C tracer analysis of uniformly labelled citrate, and analyzed the platelet proteome at different time points of storage using shotgun proteomic analysis. Alongside a literature review of PSL, this allowed us to update iAT-PLT-636 to better capture PSL metabolism. We then applied iAT-PLT-636 to describe

metabolic shifts previously shown to occur over time, in apheresis- and buffy coat-derived platelets. The models describe how changes in the extracellular medium are propagated through intracellular metabolic pathways. We investigated how the platelet nutrients acetate, glucose, glutamine, and more, contribute to the differences observed in platelet metabolism during storage from the two separate preparation methods. The results summarize and provide the most accurate biochemical description of platelet metabolism during storage in PAS to date and represent a foundation for the optimization of future platelet additive solutions and investigation of platelets metabolism ex vivo.

MATERIALS AND METHODS

Metabolite measurements

The metabolomics data sets used in this study were obtained in two separate storage experiments previously performed by our group (**Table S1**) and consist of extracellular metabolite concentrations and blood gas and hematological parameters (**Table S2**). The collection of these data sets are described in (19, 20). In both experiments the platelet concentrates (PCs) were stored in plastic containers (PL 2410, Fenwal) containing approximately 70 % T-sol storage solution (Baxter; sodium chloride 115 mM, sodium acetate 30 mM, sodium citrate dihydrate 10 mM at pH 7.2) and 30 % plasma.

The first data set consists of 8 PCs collected via the buffy coat method (BC-PCs). Each PC was produced by collecting whole blood into citrate phosphate dextrose (CPD), then separating and pooling buffy coats from five healthy donors, as described in (20). The second data set consists of measurements of 8 platelet concentrates collected by apheresis (AP-PCs) into CPD, from healthy donors, described in detail in (19).

At each time point the platelet samples were drawn from the PCs, immediately after sampling a blood gas analyzer (abl90) was used to measure glucose and lactate concentrations. The intra- and extracellular fractions where then separated by centrifugation as described before (19). The fractions were aliquoted and stored at -80°C prior to LC-MS measurements. An additional sample was drawn from the PCs at each time point and mitochondrial activity was estimated by measuring the accumulation of the membrane-permeant dye JC-1 in the platelet mitochondria using flow cytometry. Here we have expanded the analysis by measuring the extracellular concentration of acetate and citrate in the extracellular fractions.

Enzymatic assay kits were used to measure the extracellular concentrations of acetate (ACETAK) and citrate (K-CITR), according to the manufacturer's instruction (Megazyme International Ireland Ltd, Wicklow, Ireland) using a microplate reader (Spectramax M3, Molecular Devices, Sunnyvale, CA). Statistical analysis was carried out by a two-tailed paired t-test where applicable.

To account for citrate metabolism, an apheresis unit was incubated in T-Sol containing uniformly labelled ^{13}C citrate (CLM-9021-PK, Cambridge Isotope Laboratories) and compared to an untreated apheresis unit from the same donor. Unit sampling and subsequent metabolomics analysis was performed in a similar manner as previously described to determine qualitative profiles of intracellular and extracellular metabolites (21, 22). Measured intensities were corrected for natural abundance of ^{13}C-isotopes using the software Isocor (23).

Proteomic analysis

Three PC units were prepared by the buffy coat method from a pool of five healthy blood donors each, of mixed age and sex at the Blood bank, Landspitali-University Hospital, Iceland and stored as previously

reported (20). Three 4 mL samples were collected on days 1, 3 and 6 of storage. At the end of the experiment, pathogen analysis at Landspitali-University Hospital was negative. Protein isolation, peptide cleavage and purification is expanded upon **Supplementary File 1**.

Two different methods of peptide separation and mass spectrometry analysis were performed. For the first PC unit, peptide separation was achieved by one dimensional reversed phase liquid chromatography using nanoACQUITY UPLC (Waters Corporation, USA) with a 75 µm x 25 cm C18 HSS T3 column. The experiments were performed using a 1.5 hour gradient (5-40 % acetonitrile over 90 min) at a flow rate of 300 nL/min. Mass spectrometry analysis was performed using SYNAPT G2Si HDMS (Waters, Manchester UK) operating in a data-independent manner coupled with ion mobility. All samples were measured in triplicates. Protein identification and label-free quantification were performed using Progenesis QI for proteomics (NonLinear Dynamics, UK). For the second two PC units the peptides were injected and washed on a trap column (Acclaim PepMap 100 C18, 100 µM x 2 cm, Thermo Scientific), then separated on a second column (Easy-Spray PepMap RSLC C18 column, 75 µM x 50 cm, Thermo Scientific) using Ultimate 3000 RSLCnano system (Thermo Scientific) The mobile phases consisted of buffer A (0.1 % formic acid) and buffer B (80 % acetonitrile in 0.08 % formic acid), the gradient went from 2 % to 98 % buffer B in 152 minutes, followed by 18 minutes with 2 % solvent B with a with a flow rate of 300 nL/min. The samples were transferred to mass spectrometer via an Easy-Spray source with temperature set at 50˚C and a source voltage of 2.0 kV. The mass spectrometry analysis was performed using LTQ Orbitrap Velos Pro (Thermo Scientific) operating in data dependent acquisition mode. Protein identification and label-free quantifications were carried out using MaxQuant (24).

For the semi-quantitative analysis only proteins where used that were detected with both methods with at least 1 unique peptide, and a non-zero normalized intensity measured at least one time point in all three PC units. To allow for a semi-quantitative comparison from both proteomic methods, protein abundances measured within each PC where first z-score transformed. Principal component analysis (PCA) was carried out with the statistical software R version 3.4.3, hierarchical clustering analysis and heat map generation were carried out using MetaboAnalyst 3.0 (25). The Reactome knowledgebase (26) was used to sort the detected proteins by biological pathways.

A mathematical model of platelet metabolism

Based on the results obtained from the metabolite and proteomic analysis, iAT-PLT-636 metabolic reconstruction (17) was refined by adding transporters necessary for a functional malate-aspartate shuttle, mitochondrial acetate transport and acetyl-coA synthetase, pyrimidine biosynthesis, diffusion of ammonia through the mitochondrial membrane, transport of and exchange of D-lactate, and production and transport of mitochondrial phosphoenolpyruvate. The reaction catalyzed by the cytosolic form of aconitase is split into two reactions, allowing the formation of the reaction‘s intermediate cis-aconitate. Aconitate plasma membrane transport and exchange reactions were added to account for the observed aconitate secretion.

More precisely, to address gaps in the iAT-PLT-636 model, sixteen metabolic reactions (KGMALtm, ASPGLUm, CITtam, PEPtam, Lac_D_Transport, ACSm, PPAm, PPCKm, ADK1m, RPE, CBPS, ASPCT, DHORTS, DHORD_NAD, ORPT, OMPDC) were added, all of which have been detected in proteomic experiments. Also added to the model were the electroneutral diffusion of acetate across the mitochondrial membrane (ACt2m) on the grounds that the unionized form acetic acid can diffuse over lipid membranes. Further four reactions (EX_k(e), ASNS1, ASNtN1, NH4D, sink_orn[c], EX_LacD_e) where added to resolve infeasibility of the model (**Table S3**). Thirteen reactions were removed from the iAT-

PLT-636 model either due to a lack of evidence for the reactions (ACCOAtm, MALSO3tm, MALTSULtm, MALtm, LDH_D) and/or to eliminate internal loops (FBP, SUCOASm, UGLT, PFK26, GALT,PPDOx, PPDOy, SO4t4_2) (**Table S4**). Finally, the reaction ACONT, was replaced by ACONT1 and ACONT1 and aconitate transport (acontT2) and exchange (EX_acon(e)) reactions added to allow for cytosolic aconitate production (**Tables S3-S4**).

Model constraints derived from metabolomics data

Metabolomics data was used to define the boundary conditions of the models (i.e. constrain them) as follows: First the storage time was divided into three stages representative of fresh (days 1-3), intermediate (days 4-6) and expired (days 7-10) PCs, hereafter referred to as stages 1, 2 and 3 respectively.

For each of the three storage stages and each extracellular metabolite *k* included in the model, a line was fit through the corresponding data points (**Figure 1**, **Table S5**). The slope of the line, normalized to the average platelet count in each storage bag, defined the exchange flux v_k of the metabolite, with positive slope denoting secretion and negative slope denoting consumption (**Figure 1**).

In case this results in an infeasible model, i.e. no set of fluxes exist which fulfill all model constraints, the exchange fluxes are adjusted slightly to obtain a feasible model. The adjustment of exchange fluxes is determined by solving the following optimization problem (27),

$$\text{minimize } \sum_{j \in Rx} (p_j + n_j) \tag{1}$$

$$S\mathbf{v} = 0 \tag{2}$$

$$l_j - n_j \leq v_j \leq u_j + p_j \qquad j \in R_x \tag{3}$$

$$v_j \geq 0 \qquad j: l_j > 0, u_j > 0 \tag{4}$$

$$l_i \leq v_i \leq u_i \qquad i \in R_n \tag{5}$$

$$p_j \geq 0, n_j \geq 0 \qquad j \in R_x \tag{6}$$

The set of exchange reactions to be relaxed is denoted by R_x and the set R_n represents all other reactions. The objective (1) is to minimize the total adjustment to exchange fluxes by adjusting the amount of upper (p_j) and lower bound relaxations (n_j) and network fluxes (v) while fulfilling the steady state mass balance constraints (2). Constraints (3) enable relaxation of the exchange reactions. Constraints (4) prevent the uptake of metabolites that should only be secreted and constraints (5) are the usual flux balance analysis upper and lower bounds. The algorithm was implemented in Matlab (Mathworks, Natick, MA, USA) using the CVX modeling language (CVX Research 2012). The Gurobi solver (Gurobi Optimization 2017) was used to solve the optimization problem. Exchange flux alterations made to the models as a result of the optimization algorithm can be found in **Table S6**.

Model analysis

All model computations and analysis were done in the Matlab environment (Mathworks, Natick, MA, USA) using the COBRA toolbox (28). Graphical representations of reaction pathways were obtained with the Escher tool (29). Flux balance analysis (FBA) (30) was used to determine the maximal amount of ATP produced by the models described above. Random sampling (31) was then used to obtain estimates of

flux distributions in the models. ATP generation was constrained to 90 % of the maximum ATP production prior to sampling. The flux distributions are affected both by the network topology as well as the intervals containing the exchange fluxes. Average fluxes obtained by random sampling of the allowed flux space in individual reactions under different conditions were compared.

RESULTS

Acetate is the main platelet fuel during PLT storage

In this study, we set out to capture and explain key features of PSL metabolism using cell scale metabolic modelling. Extracellular metabolomics data descriptive of changes in metabolite concentration over time from our previous studies was used and formed the basis for the analysis in this study (19, 20). When present in the storage media, acetate is the primary fuel of PLTs (9). Acetate was not part of the previous metabolomics screening and to address this, we measured changes in extracellular acetate concentrations. In addition, to support previous citrate metabolomics measurements, we measured the extracellular concentration of citrate using an enzyme coupled assay. These measurements were performed on the same PLT samples as the previously published metabolomics assays (19, 20).

The rate of acetate uptake remained fairly constant over the first 7 days of storage in both AP-PCs (0.92 ± 0.12 mM/day) and BC-PCs (1.04 ± 0.07 mM/day) and decreased most between days 7 and 10. A significant decrease in acetate concentration was measured between days 1 and 7 in both AP-PC ($p = 9.3 * 10^{-7}$) and BC-PC ($p = 3.0 * 10^{-5}$). Conversely a significant change in extracellular citrate was measured only in the AP-PCs between days 1 and 10 ($p = 0.0059$), not however in BC-PCs ($p = 0.55$) (**Figure 1**).

The measured uptake rate of citrate in the AP-PCs was considerably higher than previously reported (32, 33); we therefore confirmed citrate metabolism further by adding uniformly labelled ^{13}C labeled citrate to a single AP-PC unit. Label enrichment was detected in intracellular citrate and malate, and extracellular citrate and aconitate (**Figure 2**). The enrichment of extracellular aconitate mirrored that of the extracellular citrate as opposed to the intracellular pool. This indicated that media derived citrate is converted to aconitate without mixing with the total intracellular citrate pool, possibly due to compartmentation. To account for this in the model, the reaction converting cytosolic citrate to isocitrate (ACONT) was split into its two separate reactions, one that reversibly converts citrate to aconitate (ACONT1), and one that reversibly converts aconitate to isocitrate (ACONT2). Only a small label enrichment was detected in intracellular malate, and only as the fully labelled isotopologue. The relative contribution increased from 2 % at day zero, to 7 % at day ten of storage, indicating that citrate is not metabolized via the TCA to a significant extent.

Intracellular metabolic protein abundance changes during storage

In order to account for a change in abundance of metabolic proteins during storage and their effect on PSL metabolism, we carried out shotgun proteomics analysis of three BC-PCs units at three different time points. The time points reflected the three phase metabolic decay of PSL (19, 20). The measurements were made using two different methods whose analysis was then combined as described in materials and methods. With the first method (qTOF) a total of 1663 proteins with at least one unique peptide were identified. The second method (Orbitrap) identified 2118 proteins with at least one unique peptide. A total of 882 proteins were identified with both methods. Pathway analysis identified 332 metabolic proteins of which 160 were detected with both methods, on which a semi-quantitative analysis on the protein abundances was performed. Principal component analysis revealed a distinct separation of the samples into three groups based on storage time (**Figure 3**). The majority of the

proteins contributing to the PCA separation, decreased in abundance with storage time (**Table 1**). A similar result was obtained by unsupervised hierarchical clustering (**Figure 3**). The results from the proteomic analysis by both methods can be found in the Supplementary file 2. Using these results supplemented by literature review of the platelet proteome, 16 reactions were added to the model, including reactions necessary for a functional malate-aspartate shuttle, acetate metabolism, and pyrimidine biosynthesis (**Table S3**).

Platelet metabolism was modelled as a three-phase metabolic decay using iAT-PLT-636

In order to make the model more descriptive of PSL metabolism we refined and updated iAT-PLT-636 based on the results obtained from the ^{13}C tracer and proteomic analysis, as well as through literature review (**Tables S3 and S4**). The refined model was used to analyze the PSL metabolomics data that we sectioned into three groups, representative of days 1-3 (Stage 1), days 4-6 (Stage 2), and days 7-10 (stage 3) of storage. The measured changes in extracellular metabolite concentrations within each stage were then used as boundaries to define the maximum and minimum allowed flux of metabolites through the metabolic pathways (**Figure 1**). The extracellular fluxes together with the stoichiometric coefficients of the network reconstruction therefore implicitly define fluxes in metabolic pathways. Three models descriptive of steady state metabolism in platelets during stages 1, 2 and 3 were created. Flux analysis of these models allowed the estimation of the most likely flux of metabolites through metabolic pathways and its comparison between all stages. In the following, analysis in terms of "fluxes" refers to predictions made by the PLT model, specifically referring to the arithmetic means of the randomly sampled flux values.

In order to visualize the results, flux values were mapped onto graphical representations of the platelet biochemical network. **Figure S1** shows the average flux distributions calculated for the glycolytic and pentose phosphate pathways during stage 1 in BC-PCs. The average flux values for each reaction are listed in **Supplementary File 3**. Selected metabolic features are described further below.

Buffy coat derived platelet metabolism is captured in iAT-PLT-636

The primary role of platelet metabolism is to provide energy in the form of ATP necessary to maintain homeostasis. To investigate the ATP production potential, we compared the metabolism between the stages of BC-PCs by FBA. This analysis predicted a roughly 1.5-fold increase in maximal ATP turnover rate between stages 1 and 2 with a decline in ATP turnover rate during stage 3 (**Table 2**). The contribution towards ATP production from glycolysis and the oxidative phosphorylation was constant during the first two stages with 11-13 % of ATP produced via glycolysis and the remaining 87-89 % in the mitochondria. In stage 3, however, the relative contribution of glycolysis increased as the flux through oxidative metabolism decreased (**Table 3**, **Figure 4 A-B**). Previous experiments have estimated 15-30 % ATP turnover derives from glycolysis with the remainder from oxidative phosphorylation (34-37). In accordance with energy production, the oxygen consumption rate was predicted to increase between the first two stages and decrease in stage 3, with a parallel change in CO_2 production (**Table 2**). To reveal further how specific nutrients, contribute to these storage metabolic phenotypes, we investigated the main contributors to platelet metabolism during storage.

Decreased acetate oxidation and increased glycolysis, PPP and polyol pathway flux accompany PSL

During storage in acetate containing media, ATP is primarily produced from the catabolism of acetate and glucose, with a minor contribution from glutamine and citrate. Accordingly, in the BC-PC model, citrate and glutamine maximally accounted for 5.4-10.3 % of O_2 consumption combined (**Table 4**).

Acetate, however, contributed most to O_2 consumption. Nearly all consumed acetate (~99 %) was predicted to be converted to acetyl-coA via the acetyl-coA synthetase reaction in the mitochondria where it was predicted to be fully oxidized to CO_2. Acetate oxidation was predicted to contribute to 83 % of total ATP production during stage 1, 73 % during stage 2, and 58 % during stage 3. Negligible amounts of acetate were predicted to be incorporated into fatty acids, consistent with low amounts of acetate incorporation into platelets measured in ^{14}C tracer studies (9, 38).

Glucose was the second largest source of energy during storage and the only source for ATP production in the cytosol. The majority of glucose (86-98 %) was converted to lactate via aerobic glycolysis with 2-11 % of glucose-6-phosphate predicted to enter the pentose phosphate pathway (PPP) (**Table 5**). To allow comparison to classical ^{14}C studies (9, 34, 39, 40) we calculated the proportion of glucose carbons converted to CO_2 (**Table 5**). Assuming that all acetyl-coA formed from pyruvate was fully oxidized, the percentage of glucose derived CO_2 was predicted to be: 0.8 % for stage 1, 7.7 % for stage 2, and 7.3 % for stage 3. Notably, the increase in glucose derived CO_2 between stages 1 and 2 was not only due to an increase of flux through the pyruvate dehydrogenase reaction and consequent oxidation in mitochondria, but also due to increased flux through the PPP. Analysis of model reaction flux showed that the increase through the PPP was driven by glucose entering the polyol pathway. Specifically, during stage 2, 44 % of glucose taken up by the platelets was predicted to be funneled through aldose reductase creating an increased demand for NADPH. Metabolic network analysis thus identified this reaction accounting for the increase of flux into the PPP in stage 2 (**Table 5**).

Apheresis derived PC have different metabolic storage profiles than buffy coat PC

A different metabolic profile was observed in AP-PCs compared to BC-PCs. Comparison of the models indicated that during the first two stages, glycolysis and pyruvate oxidation were more active in the AP-PCs, with less energy deriving from acetate oxidation (**Tables 2-4**). The increase in energy production between stages 1 and 2 was comparatively small in AP-PCs compared to BC-PCs (**Figure 4**). The rate of glucose derived pyruvate oxidation was predicted to increase substantially between the first two stages in both conditions (**Table 5**). However, between stages 2 and 3 the energy production decreased in both conditions; but this decrease was more substantial in the AP-PCs, with the ATP turnover rate predicted to decrease by more than 40 %. The acetate uptake rate decreased by roughly 50 % between stages 2 and 3 in both conditions. This decrease had a larger impact on the AP-PCs, as glucose was completely depleted in or before stage 3. Glycolysis is therefore unable to compensate for the decrease in acetate consumption resulting in a lower ATP turnover rate in AP-PC platelets.

Glutamine and citrate can both compensate for lower pyruvate oxidation by generating acetyl-CoA via the TCA cycle. Measured glutamine uptake rate was substantially lower in AP-PCs compared to BC-PCs, resulting in a predicted lower rate of ammonia accumulation. The citrate uptake was however considerably higher in AP-PCs as compared to BC-PCs, in stages one and three (**Table 2**).

DISCUSSION

Recent studies have shown a correlation between platelet age and transfusion outcome (41). Metabolism is one important contributor to PSL and can be manipulated to enhance the quality of platelets during storage through targeted changes of platelet storage media. Employing metabolomics and standard platelet quality control screening, we previously monitored over 150 parameters in BC-PCs and AP-PCs. Here we addressed gaps in this dataset to more accurately define platelet metabolism under storage conditions. The majority proportion of platelet energy is derived from oxidative metabolism with acetate being the preferred fuel when present in PAS (34). Given the high

concentration of acetate in T-Sol, a measure of acetate uptake was imperative for investigating and modeling platelet energy metabolism. Acetate was consumed over the duration of storage in both BC-PCs and AP-PCs at a rate comparable to previously reported values (42, 43) (**Figure 1**), (**Table 2**). Comparison of buffy coat and apheresis acetate consumption rates show that individual variation does not markedly influence the ability to metabolize acetate (**Figure 1**).

The data from our previous study indicated that citrate might contribute significantly to platelet central carbon metabolism (19). The measured change in citrate concentration over time was however not statistically significant, possibly due to low precision of our LC-MS measurements. We aimed to accurately account for major carbon contributing nutrients within iAT-PLT-636 and therefore re-measured the citrate during storage which showed a significant drop in citrate concentration during storage in AP-PCs only (**Table 1**). ^{13}C tracer analysis, of citrate in T-Sol with uniformly labeled ^{13}C citrate, confirmed its metabolism in apheresis derived platelets. The lack of intracellular citrate and malate isotopologues, other than uniformly labeled, however, suggest that little, if any, citrate is metabolized within the mitochondria, but rather metabolized to malate within the cytosol during storage. This is consistent with reduced citrate contribution to CO_2 production in platelets in the presence of acetate (32). Combined with the acetate and citrate measurements reported here, our previous metabolomics data quantitatively define the extracellular metabolic changes of PSL. In order to better understand how changes in extracellular nutrients combine and contribute to and maintain intracellular energy homeostasis in PLTs during storage, we adopted a metabolic systems biology approach. It was necessary to modify iAT-PLT-636 for a more accurate interpretation of platelet metabolism during storage. These modifications allowed improved modelling of the main PLT nutrients, glucose, acetate, and glutamine/glutamate oxidation within iAT-PLT-636, on account of the addition of reactions related to aspartate malate shuttle, acetate metabolism, ammonia, and more (**Tables S3-S4**). A literature review highlighted the ambiguous and variable experimental conditions from which platelet metabolic knowledge during storage originates, which is apparent from the broad range of metabolic fluxes during storage reported in the literature (**Table 2**). The modified model of PLT metabolism during storage represents a framework in which to define and interpret platelet metabolism.

BC-PCs platelets exhibit discrete metabolic phenotypes that represent fresh, intermediate, and expired PLTs that correlate with activation markers including GpIIb/P-selectin, sP-selectin, and sCD40L (19, 20). For comparative purposes, we modelled PSL as a three-phase decay. Systems analysis of buffy coat and apheresis platelet metabolic data using iAT-PLT-636 predicted that the requirement to produce ATP was different and reflected changes in measured nutrient utilization over time. Not surprisingly, glucose and acetate uptake, a measure of glycolytic and TCA cycle activity respectively within iAT-PLT-636, were responsible for the largest quantitative differences to intracellular metabolic pathway flux in platelets irrespective of collection procedure (**Tables 2 and 4**). Both models predicted a near full oxidation of acetate and decreased acetate consumption during storage in both AP-PC and BC-PC which is reflected in the decreased contribution of acetate to total oxygen consumption between stages. This result is in good agreement with a recently published study (44) where the capacity for acetate incorporation into the acetyl-CoA was shown to decrease considerably during storage.

Most of the ATP generation in platelets takes place in the mitochondria [18]. The metabolic models of platelet metabolism are consistent with previous reports on PSL metabolism. Prediction and literature values are compared in Tables 2, 4 and 5. Overall, model predictions correspond with previous literature values although some variability is to be expected given different platelet preparation methods, storage conditions, and experimental setup. In previous reports, ATP production by glycolysis was assumed to be stoichiometric with lactate secretion resulting in the overestimation of mitochondrial ATP production as a constant P/O value (moles ATP produced per moles O_2 reduced by the electron transport chain) was used and the cost of acetyl-coA synthesis from acetate was not factored into calculations (34-37). Here we have determined how the uptake of metabolic fuels is propagated during storage over time with

better pathway resolution than previously reported. Our results define PSL metabolic changes on the systems level, the functional consequences of which are activated platelets that represent lesser quality transfusion products (6). It must be noted that the lack of lipid measurement, and therefore, lack of constraints to lipid metabolism in the models presents a limitation to this study. Human platelets do oxidize lipids (45), however, with high concentration of acetate is in the media, lipid oxidation has been reported to account for only a negligible proportion of the total oxygen consumption (34).

The proteomic analysis allowed us to investigate whether the changes in metabolic activities are dictated by the changes to the abundances of metabolic proteins. With our analysis we concluded that most of the metabolic enzyme either decrease in abundance or remain stable over the duration of the storage time. Furthermore no obvious increase or decrease of protein abundances was observed within distinct metabolic pathways. This led us to the conclusion that global changes in metabolic protein abundances are not a major driving force behind the observed changes in the platelet metabolism during storage. This is in good agreement with Rijkers et al. (46) where only 21 out of the 2501 quantified proteins changed significantly in during 16 days of storage measured in three BC-PCs, of which 18 decreased in abundance over time.

iAT-PLT-636 can be utilized as a hypothesis generator. Acetate addition to platelet storage counteracts lactate induced acidification of platelet media during storage (9) and although lowering acetate concentration influences ATP maintenance, ATP has been found to be only weakly correlated with platelet viability (47). Analysis of metabolic data with iAT-PLT-636 highlights alternative routes that may be pursued to counteract PSL. Flux alterations in glycolysis and the TCA cycle influenced the oxidation of glutamine and citrate differently based upon the collection method. In particular, citrate was more actively metabolized in AP-PCs. Citrate oxidation was allowed in our models to take into account previous reports (32), but was low compared to other oxidative fuels. The models suggest that glutamine and to a lesser degree citrate can contribute to ATP production and may serve as alternative ATP sources, with their efficacy being dependent upon the PLT production method and media composition (e.g. inclusion of acetate).

In addition to ATP, the models account for ammonium production that influences intracellular pH. Ammonium is primarily derived from glutamine in platelets, and model prediction of potential maximal glutamine oxidation to CO_2 were comparable to literature values (48). The models predicted ammonia accumulation during storage with a rate of 0.019-0.10 mmol/day/10^{12} plts (**Table 2**). Ammonia originates mostly from glutaminolysis (63.5-80.8 %) and purine degradation (14.3-33.9 %) with the remainder coming from asparagine metabolism (1.0-3.7%) (**Table S7**). Ammonia secretion is predicted to be higher in BC-PC in all stages, on account of higher uptake rate of glutamine.

Generation of the reducing equivalent NADPH was predicted to take place primarily in the cytosol. The percentage of total glucose shunted into the PPP during storage in T-Sol was 1.9-11.3 % and contributed to 18-30 % of the total cellular NADPH turnover (**Table S8**). PPP activity in platelets has previously been estimated from labeled carbon experiments and estimates vary considerably, ranging from 1 % of the glucose uptake (39, 40) to 20 % (9). The largest contribution to NADPH turnover is predicted to be the cytosolic isocitrate dehydrogenase reaction that accounted for 55-67 % of the total NADPH turnover with its mitochondrial counterpart contributing to 6-11 % of the NADPH turnover.

Changes to NADPH turnover rate during storage were found to correlate to flux through the polyol pathway. The models predict a considerable percentage of glucose to be utilized by the polyol pathway (9-44 %) (**Table 5**). Under euglycemic conditions approximately 3 % of glucose is utilized by the polyol pathway in human erythrocytes (49). In the rapid lens this ratio has been demonstrated to reach approximately 30 % under hyperglycemic conditions (50). In human platelets the activity and abundance of aldose reductase (AR), the enzyme catalyzing the first and rate limiting step of the polyol pathway, increases upon activation with collagen (51) and by activating glycoprotein VI with a specific monoclonal antibody (52). Furthermore it has been demonstrated that AR plays an important role in transducing

collagen signaling in platelets (51) and is involved in oxidative stress associated activation of p38 mitogen activated protein kinase (MAPK p38α) that has been strongly associated with PSL (53, 54). In light of these results, our modelling analysis suggest that flux through the polyol pathway increases during PSL in connection to enhanced glycolysis on account of mitochondrial dysfunction and suppressed ability to generate ATP.

Targeted media manipulation focused upon these metabolic pathways and aimed at alternating carbon, ammonia, and NAPDH precursors may provide opportunities to manipulate intracellular pH and counteract oxidative stress. With prolonged storage, platelets indeed show signs of mitochondrial dysfunction (**Figure 1**) (55) that are coupled to formation of the mitochondrial permeability transition pore and programmed cell death (56). Disruption of oxidative metabolism increases the rate of glycolysis to compensate for a decrease in ATP turnover (57). The decrease in oxidative metabolism in long term stored platelets has previously been demonstrated (58). We have described the shifts in metabolic pathway utilization that take place in buffy coat and apheresis platelets during storage through cell scale modelling. We conclude that future platelet additive solutions should focus on manipulation of biophysical properties such as temperature, pH, and ionic strength such as to minimize the initialization of mechanisms that result in activation and apoptosis. Multiple platelet additive solutions have been formulated with these parameters in mind (59), however few have managed to optimize both biochemical and biophysical properties simultaneously. The models that we have described here represent steps towards this goal.

Acknowledgements

This work was supported by a University of Iceland PhD grant, RANNIS grant no. 130591-051 and the European Research Council grant proposal no. 232816. The authors thank the staff at the Blood bank and at the Center for System Biology at the University of Iceland along with Dr. Joanne Connolly and Douglas Lamont for technical support.

Conflicts of interest

BOP is the co-founder of Sinopia biosciences.

Author Contributions

FJ performed the experiments, analyzed the data and wrote the paper. GP, SG, BOP and OES designed the experiments and contributed to writing the paper. SG analyzed the data, designed the experiment and wrote the paper. OR designed the experiments and wrote the paper.

References

1. Zucker MB, Nachmias VT. Platelet activation. Arteriosclerosis (Dallas, Tex). 1985;5(1):2-18.
2. Gawaz M, Langer H, May AE. Platelets in inflammation and atherogenesis. The Journal of clinical investigation. 2005;115(12):3378-84.
3. Seghatchian J, Krailadsiri P. The platelet storage lesion. Transfusion medicine reviews. 1997;11(2):130-44.
4. Devine DV, Serrano K. The platelet storage lesion. Clinics in laboratory medicine. 2010;30(2):475-87.
5. Mittal K, Kaur R. Platelet storage lesion: An update. Asian Journal of Transfusion Science. 2015;9(1):1-3.
6. Sahler J, Grimshaw K, Spinelli SL, Refaai MA, Phipps RP, Blumberg N. Platelet storage and transfusions: new concerns associated with an old therapy. Drug discovery today Disease mechanisms. 2011;8(1-2):e9-e14.
7. Murphy S, Gardner FH. Platelet storage at 22 degrees C: role of gas transport across plastic containers in maintenance of viability. Blood. 1975;46(2):209-18.
8. Gulliksson H, Sallander S, Pedajas I, Christenson M, Wiechel B. Storage of platelets in additive solutions: a new method for storage using sodium chloride solution. Transfusion. 1992;32(5):435-40.
9. Murphy S. The oxidation of exogenously added organic anions by platelets facilitates maintenance of pH during their storage for transfusion at 22 degrees C. Blood. 1995;85(7):1929-35.
10. Gulliksson H. Storage of platelets in additive solutions: the effect of citrate and acetate in in vitro studies. Transfusion. 1993;33(4):301-3.
11. Gulliksson H. Defining the optimal storage conditions for the long-term storage of platelets. Transfusion medicine reviews. 2003;17(3):209-15.
12. McCullough J, Goldfinger D, Gorlin J, Riley WJ, Sandhu H, Stowell C, et al. Cost implications of implementation of pathogen-inactivated platelets. Transfusion. 2015;55(10):2312-20.
13. Zimring JC, Slichter S, Odem-Davis K, Felcyn JR, Kapp LM, Bell LN, et al. Metabolites in stored platelets associated with platelet recoveries and survivals. Transfusion. 2016;56(8):1974-83.
14. O'Brien EJ, Monk JM, Palsson BO. Using Genome-scale Models to Predict Biological Capabilities. Cell. 2015;161(5):971-87.
15. Agren R, Mardinoglu A, Asplund A, Kampf C, Uhlen M, Nielsen J. Identification of anticancer drugs for hepatocellular carcinoma through personalized genome-scale metabolic modeling. Molecular systems biology. 2014;10(3).
16. Bordbar A, Palsson BO. Using the reconstructed genome-scale human metabolic network to study physiology and pathology. Journal of internal medicine. 2012;271(2):131-41.
17. Thomas A, Rahmanian S, Bordbar A, Palsson B, Jamshidi N. Network reconstruction of platelet metabolism identifies metabolic signature for aspirin resistance. Scientific Reports. 2014;4.
18. Bordbar A, Yurkovich JT, Paglia G, Rolfsson O, Sigurjonsson OE, Palsson BO. Elucidating dynamic metabolic physiology through network integration of quantitative time-course metabolomics. Scientific reports. 2017;7:46249.
19. Paglia G, Sigurjonsson OE, Rolfsson O, Valgeirsdottir S, Hansen MB, Brynjolfsson S, et al. Comprehensive metabolomic study of platelets reveals the expression of discrete metabolic phenotypes during storage. Transfusion. 2014;54(11):2911-23.
20. Paglia G, Sigurjonsson OE, Rolfsson O, Hansen MB, Brynjolfsson S, Gudmundsson S, et al. Metabolomic analysis of platelets during storage: a comparison between apheresis- and buffy coat-derived platelet concentrates. Transfusion. 2015;55(2):301-13.
21. Rolfsson Ó, Sigurjonsson ÓE, Magnusdottir M, Johannsson F, Paglia G, Guðmundsson S, et al. Metabolomics comparison of red cells stored in four additive solutions reveals differences in citrate anticoagulant permeability and metabolism. Vox sanguinis. 2017;112(4):326-35.
22. Rolfsson Ó, Johannsson F, Magnusdottir M, Paglia G, Sigurjonsson ÓE, Bordbar A, et al. Mannose and fructose metabolism in red blood cells during cold storage in SAGM. Transfusion.n/a-n/a.

23. Millard P, Letisse F, Sokol S, Portais JC. IsoCor: correcting MS data in isotope labeling experiments. Bioinformatics (Oxford, England). 2012;28(9):1294-6.
24. Cox J, Mann M. MaxQuant enables high peptide identification rates, individualized p.p.b.-range mass accuracies and proteome-wide protein quantification. Nature Biotechnology. 2008;26:1367.
25. Xia J, Sinelnikov IV, Han B, Wishart DS. MetaboAnalyst 3.0—making metabolomics more meaningful. Nucleic acids research. 2015;43(W1):W251-W7.
26. Fabregat A, Sidiropoulos K, Garapati P, Gillespie M, Hausmann K, Haw R, et al. The Reactome pathway Knowledgebase. Nucleic acids research. 2016;44(D1):D481-7.
27. Halldorsson S, Rohatgi N, Magnusdottir M, Choudhary KS, Gudjonsson T, Knutsen E, et al. Metabolic re-wiring of isogenic breast epithelial cell lines following epithelial to mesenchymal transition. Cancer Letters. 2017;396:117-29.
28. Schellenberger J, Que R, Fleming RM, Thiele I, Orth JD, Feist AM, et al. Quantitative prediction of cellular metabolism with constraint-based models: the COBRA Toolbox v2.0. Nat Protoc. 2011;6(9):1290-307.
29. King ZA, Dräger A, Ebrahim A, Sonnenschein N, Lewis NE, Palsson BO. Escher: A Web Application for Building, Sharing, and Embedding Data-Rich Visualizations of Biological Pathways. PLOS Computational Biology. 2015;11(8):e1004321.
30. Orth JD, Thiele I, Palsson BO. What is flux balance analysis? Nat Biotech. 2010;28(3):245-8.
31. Schellenberger J, Palsson BO. Use of randomized sampling for analysis of metabolic networks. J Biol Chem. 2009;284(9):5457-61.
32. Cartledge S, Candy DJ, Hawker RJ. Citrate metabolism by human platelets. Transfusion medicine (Oxford, England). 1997;7(3):211-5.
33. Niu X, Whisson ME, Guppy M. Types and sources of fuels for platelets in a medium containing minimal added fuels and a low carryover plasma. British journal of haematology. 1997;97(4):908-16.
34. Guppy M, Whisson ME, Sabaratnam R, Withers P, Brand K. Alternative fuels for platelet storage: a metabolic study. Vox sanguinis. 1990;59(3):146-52.
35. Kilkson H, Holme S, Murphy S. Platelet metabolism during storage of platelet concentrates at 22 degrees C. Blood. 1984;64(2):406-14.
36. Niu X, Arthur P, Abas L, Whisson M, Guppy M. Carbohydrate metabolism in human platelets in a low glucose medium under aerobic conditions. Biochimica et biophysica acta. 1996;1291(2):97-106.
37. Guppy M, Abas L, Neylon C, Whisson ME, Whitham S, Pethick DW, et al. Fuel choices by human platelets in human plasma. The FEBS Journal. 1997;244(1):161-7.
38. Shimizu T, Murphy S. Roles of acetate and phosphate in the successful storage of platelet concentrates prepared with an acetate-containing additive solution. Transfusion. 1993;33(4):304-10.
39. Murphy S, Gardner FH. Platelet storage at 22°C; metabolic, morphologic, and functional studies. The Journal of clinical investigation. 1971;50(2):370-7.
40. Baker JM, Candy DJ, Hawker RJ. Influences of pH on human platelet metabolism. Platelets. 2001;12(6):333-42.
41. Kreuger AL, Caram-Deelder C, Jacobse J, Kerkhoffs JL, van der Bom JG, Middelburg RA. Effect of storage time of platelet products on clinical outcomes after transfusion: a systematic review and meta-analyses. Vox sanguinis. 2017;112(4):291-300.
42. Johnson L, Schubert P, Tan S, Devine DV, Marks DC. Extended storage and glucose exhaustion are associated with apoptotic changes in platelets stored in additive solution. Transfusion. 2016;56(2):360-8.
43. van der Meer PF, Kerkhoffs JL, Curvers J, Scharenberg J, de Korte D, Brand A, et al. In vitro comparison of platelet storage in plasma and in four platelet additive solutions, and the effect of pathogen reduction: a proposal for an in vitro rating system. Vox sanguinis. 2010;98(4):517-24.

44. Sims C, Salliant N, Worth AJ, Parry R, Mesaros C, Blair IA, et al. Metabolic tracing analysis reveals substrate-specific metabolic deficits in platelet storage lesion. Transfusion. 2017;57(11):2683-9.
45. Slatter DA, Aldrovandi M, O'Connor A, Allen SM, Brasher CJ, Murphy RC, et al. Mapping the Human Platelet Lipidome Reveals Cytosolic Phospholipase A2 as a Regulator of Mitochondrial Bioenergetics during Activation. Cell metabolism. 2016;23(5):930-44.
46. Rijkers M, van den Eshof BL, van der Meer PF, van Alphen FPJ, de Korte D, Leebeek FWG, et al. Monitoring storage induced changes in the platelet proteome employing label free quantitative mass spectrometry. Scientific Reports. 2017;7(1):11045.
47. Holme S. Storage and Quality Assessment of Platelets. Vox sanguinis. 1998;74(S2):207-16.
48. Murphy S, Munoz S, Parry-Billings M, Newsholme E. Amino acid metabolism during platelet storage for transfusion. British journal of haematology. 1992;81(4):585-90.
49. Morrison AD, Clements RS, Travis SB, Oski F, Winegrad AI. Glucose utilization by the polyol pathway in human erythrocytes. Biochemical and Biophysical Research Communications. 1970;40(1):199-205.
50. González RG, Barnett P, Aguayo J, Cheng H-M, Chylack LT. Direct Measurement of Polyol Pathway Activity in the Ocular Lens. Diabetes. 1984;33(2):196-9.
51. Tang WH. Glucose and collagen regulate human platelet activity through aldose reductase induction of thromboxane. 2011;121(11):4462-76.
52. Schulz C, Leuschen NV, Fröhlich T, Lorenz M, Pfeiler S, Gleissner CA, et al. Identification of novel downstream targets of platelet glycoprotein VI activation by differential proteome analysis: implications for thrombus formation. Blood. 2010;115(20):4102-10.
53. Skripchenko A. An Inhibition of p38 Mitogen Activated Protein Kinase Delays the Platelet Storage Lesion. 2013;8(8).
54. Canault M, Duerschmied D, Brill A, Stefanini L, Schatzberg D, Cifuni SM, et al. p38 mitogen-activated protein kinase activation during platelet storage: consequences for platelet recovery and hemostatic function in vivo. Blood. 2010;115(9):1835-42.
55. Albanyan A-M, Harrison P, Murphy MF. Markers of platelet activation and apoptosis during storage of apheresis- and buffy coat–derived platelet concentrates for 7 days. Transfusion. 2009;49(1):108-17.
56. Leytin V, Allen DJ, Mutlu A, Gyulkhandanyan AV, Mykhaylov S, Freedman J. Mitochondrial control of platelet apoptosis: effect of cyclosporin A, an inhibitor of the mitochondrial permeability transition pore. Lab Invest. 2009;89(4):374-84.
57. Guppy M, Abas L, Arthur PG, Whisson ME. The Pasteur effect in human platelets: implications for storage and metabolic control. British journal of haematology. 1995;91(3):752-7.
58. Ravi S, Chacko B, Kramer PA, Sawada H, Johnson MS, Zhi D, et al. Defining the effects of storage on platelet bioenergetics; the role of increased proton leak. Biochimica et biophysica acta. 2015;1852(11):2525-34.
59. Gulliksson H. Platelet storage media. Vox sanguinis. 2014;107(3):205-12.
60. Zhang JG, Carter CJ, Culibrk B, Devine DV, Levin E, Scammell K, et al. Buffy-coat platelet variables and metabolism during storage in additive solutions or plasma. Transfusion. 2008;48(5):847-56.
61. Holme S, Heaton WA, Courtright M. Platelet storage lesion in second-generation containers: correlation with platelet ATP levels. Vox sanguinis. 1987;53(4):214-20.
62. Klinger MH, Josch M, Kluter H. Platelets stored in a glucose-free additive solution or in autologous plasma--an ultrastructural and morphometric evaluation. Vox sanguinis. 1996;71(1):13-20.
63. Hornsey VS, McColl K, Drummond O, McMillan L, Morrison A, Morrison L, et al. Extended storage of platelets in SSP platelet additive solution. Vox sanguinis. 2006;91(1):41-6.
64. Murphy S, Shimizu T, Miripol J. Platelet storage for transfusion in synthetic media: further optimization of ingredients and definition of their roles. Blood. 1995;86(10):3951-60.

65. Edenbrandt CM, Murphy S. Adenine and guanine nucleotide metabolism during platelet storage at 22 degrees C. Blood. 1990;76(9):1884-92.
66. Ukrainski CT, Goldfinger D, Pomerance JJ, Lee HC, Farber S, Sanchez R. Ammonia accumulation in platelet concentrates during storage. Transfusion. 1981;21(1):113-7.

Tables

Table 1. The top 25 metabolic proteins influencing the PCA separation. The proteins either increased in abundance during storage (arrow up), or decreased (arrow down) in all three PC units.

Gene ID	Change in abundance	Name
TALDO1	↓	Transaldolase
SLC25A3	↓	Phosphate carrier protein, mitochondrial
PIK3CG	↑	Phosphatidylinositol 4,5-bisphosphate 3-kinase catalytic subunit gamma isoform
SLC25A5	↓	ADP/ATP translocase 2
RDH11	↓	Retinol dehydrogenase 11
RENBP	↓	N-acylglucosamine 2-epimerase
ENO1	↓	Alpha-enolase
GPD2	↓	Glycerol-3-phosphate dehydrogenase, mitochondrial
IDH2	↓	Isocitrate dehydrogenase [NADP], mitochondrial
GRHPR	↓	Glyoxylate reductase/hydroxypyruvate reductase
LDHA	↓	L-lactate dehydrogenase A chain
PGM1	↓	Phosphoglucomutase-1
UGP2	↓	UTP-glucose-1-phosphate uridylyltransferase
ETFA	↑	Electron transfer flavoprotein subunit alpha, mitochondrial
GSTO1	↓	Glutathione S-transferase omega-1
GLO1	↓	Lactoylglutathione lyase
PYGL	↓	Glycogen phosphorylase, liver form
PGLS	↓	6-phosphogluconolactonase
HADH	↓	Hydroxyacyl-coenzyme A dehydrogenase, mitochondrial
DECR1	↓	2,4-dienoyl-CoA reductase, mitochondrial
PSAP	↓	Prosaposin
PGK1	↓	Phosphoglycerate kinase 1
ATP5L	↓	ATP synthase subunit g
FDPS	↓	Farnesyl pyrophosphate synthase
PRDX3	↓	Thioredoxin-dependent peroxide reductase, mitochondrial

Table 2. Measured and predicted values of uptake/secretion rates measured in mmol/day/10^{12} plts during stage 1 (days 1-3), stage 2 (days 4-6) and stage 3 (days 7-10) of storage. Positive values represent metabolite secretion, negative values uptake. Literature sourced experimental values vary considerably on account of various experimental conditions and are in some cases quite different from the conditions used in this study. The data are expressed as mean ± standard error of the mean.

Metabolite	Condition	Stage 1	Stage 2	Stage 3	Literature values	References
Glucose	BC-PC	-0.46 ± 0.39	-0.62 ± 0.38	-0.70 ± 0.20	-(0.16–1.3)	(9, 10, 35, 38, 42, 43, 60-63)
	AP-PC	-0.64 ± 0.24	-0.65 ± 0.28	-0.32 ± 0.12		
Lactate	BC-PC	0.90 ± 0.19	1.07 ± 0.24	1.27 ± 0.27	0.3–2.8	(9, 10, 35, 38, 42, 43, 60, 61, 63)
	AP-PC	1.19 ± 0.24	1.11 ± 0.37	0.57 ± 0.23		
Acetate	BC-PC	-0.95 ± 0.95	-1.20 ± 0.81	-0.64 ± 0.64	-(0.5–2.8)	(9, 32, 38, 42, 64)
	AP-PC	-0.82 ± 0.43	-0.80 ± 0.54	-0.42 ± 0.38		
Glutamine	BC-PC	-0.027 ± 0.29	-0.038 ± 0.029	-0.029 ± 0.012	-(0.1)	(48)
	AP-PC	-0.0072 ± 0.019	-0.0086 ± 0.0097	-0.0054 ± 0.0057		
Citrate	BC-PC	-0.0075 ± 0.42	0.034 ± 0.41	-0.019 ± 0.28	-(0–0.007)	(32, 33)
	AP-PC	-0.041 ± 0.26	0.0097 ± 0.27	-0.034 ± 0.18		
O_2*	BC-PC	-2.00 ± 0.01	-2.91 ± 0.08	-1.77 ± 0.01	-(0.76–1.96)	(9, 10, 33, 35, 38, 61, 64)
	AP-PC	-2.09 ± 0.03	-2.17 ± 0.04	-1.22 ± 0.01		
CO_2*	BC-PC	1.94 ± 0.01	2.72 ± 0.05	1.63 ± 0.01	N.A.	
	AP-PC	2.07 ± 0.03	2.08 ± 0.02	1.23 ± 0.01		
Ammonia*	BC-PC	0.080 ± 0.0007	0.100 ± 0.002	0.080 ± 0.002	0.04–0.15	(33, 65, 66)
	AP-PC	0.026 ± 0.0004	0.023 ± 0.0008	0.019 ± 0.0003		
Max ATP (FBA)	BC-PC	7.33	10.75	7.31	N.A.	
	AP-PC	8.27	8.60	4.85		
Net ATP**	BC-PC	7.00 ± 0.02	9.76 ± 0.14	7.08 ± 0.03	N.A.	
	AP-PC	7.83 ± 0.06	8.05 ± 0.07	4.70 ± 0.02		

*Model Predictions

** See supplementary text the definition of Net ATP.

Table 3. Partition of energy productions during stage 1 (days 1-3), stage 2 (days 4-6) and stage 3 (days 7-10) of storage, as predicted by the models reported as the percentage of ATP produced in mitochondria. The remaining ATP is generated in the cytosol via glycolysis. Three different methods to estimate the percentage of ATP produced in mitochondria compared. Flux balance analysis (FBA), Net ATP, and P/O ratio. See supplementary text for definitions.

Method	Condition	Stage 1	Stage 2	Stage 3	Literature values	References
FBA (%)	BC-PC	87.2	88.7	80.9	N.A.	N.A.
	AP-PC	83.8	84.7	85.8		
Net ATP (%)	BC-PC	87.1 ± 0.5	88.7 ± 2.1	80.8 ± 0.6	N.A.	N.A.
	AP-PC	83.7 ± 1.1	84.6 ± 1.3	85.8 ± 0.6		
P/O (%)	BC-PC	92.4 ± 1.0	93.7 ± 3.9	88.4 ± 1.1	70-80	(34-37)
	AP-PC	90.6 ± 2.2	91.5 ± 2.6	92.2 ± 1.2		

Table 4. The maximal contribution of selected metabolites to oxygen consumption during stage 1 (days 1-3), stage 2 (days 4-6) and stage 3 (days 7-10) of storage. The maximal contribution to oxygen consumption is defined such that the given metabolite is fully oxidized to CO_2 and all oxygen consumption is mitochondrial. The data are expressed as mean ± standard deviation.

Metabolite	Condition	Stage 1	Stage 2	Stage 3	Literature values	References
Acetate (%)	BC-PC	95.0 ± 1.3	82.6 ± 10.0	72.0 ± 0.9	85–106	(34, 38)
	AP-PC	77.5 ± 2.8	73.7 ± 3.4	65.8 ± 0.4		
Glucose (%)	BC-PC	1.1 ± 2.4	9.7 ± 31.8	17.3 ± 4.2	4.7-8.8	(37)
	AP-PC	16.6 ± 10.6	22.5 ± 12.9	26.5 ± 1.9		
Glutamine (%)	BC-PC	5.4 ± 0.03	5.2 ± 0.04	6.6 ± 0.03	10	(48)
	AP-PC	1.40 ± 0.01	1.60 ± 0.01	1.8 ± 0.01		
Citrate (%)	BC-PC	0.03 ± 0.0002	0	3.7 ± 0.02	N.A.	
	AP-PC	9.84 ± 0.12	0	15.9 ± 0.03		

Table 5. Predicted glucose utilization during stage 1 (days 1-3), stage 2 (days 4-6) and stage 3 (days 7-10) of storage. The proportion of total glucose derived carbons oxidized to CO_2 (Glucose oxidized). The proportion of glucose entering the pentose phosphate pathway (PPP). The percentage of glucose carbons metabolized via aerobic glycolysis. The percentage of glucose carbons entering the mitochondria via pyruvate dehydrogenase (PDH). The percentage of glucose entering the polyol pathway (Polyol). The data are expressed as mean ± standard deviation.

	Condition	Stage 1	Stage 2	Stage 3	Literature values	References
Glucose oxidized (%)	BC-PC	0.8 ± 0.6	7.7 ± 6.7	7.3 ± 1.7	1-12	(9, 34)
	AP-PC	9.1 ± 3.2	12.6 ± 3.8	16.7 ± 0.5		
PPP (%)	BC-PC	1.9 ± 1.3	11.3 ± 8.8	2.0 ± 1.7	1-20	(9, 39, 40)
	AP-PC	4.8 ± 3.7	5.6 ± 4.5	2.8 ± 2.3		
Aerobic Glycolysis (%)	BC-PC	98.0 ± 0.3	86.1 ± 1.5	90.8 ± 0.2	N.A.	
	AP-PC	92.8 ± 0.6	85.3 ± 0.7	87.7 ± 0.3		
PDH flux (%)	BC-PC	0.5 ± 0.2	5.8 ± 1.5	6.9 ± 0.3	N.A.	
	AP-PC	5.8± 0.7	11.7 ± 0.8	12.0 ± 0.4		
Polyol (%)	BC-PC	12.5 ± 7.9	44.0 ± 22.8	8.9 ± 5.5	N.A.	
	AP-PC	20.7 ± 12.4	23.8 ± 14.1	12.2 ± 7.7		

Figures

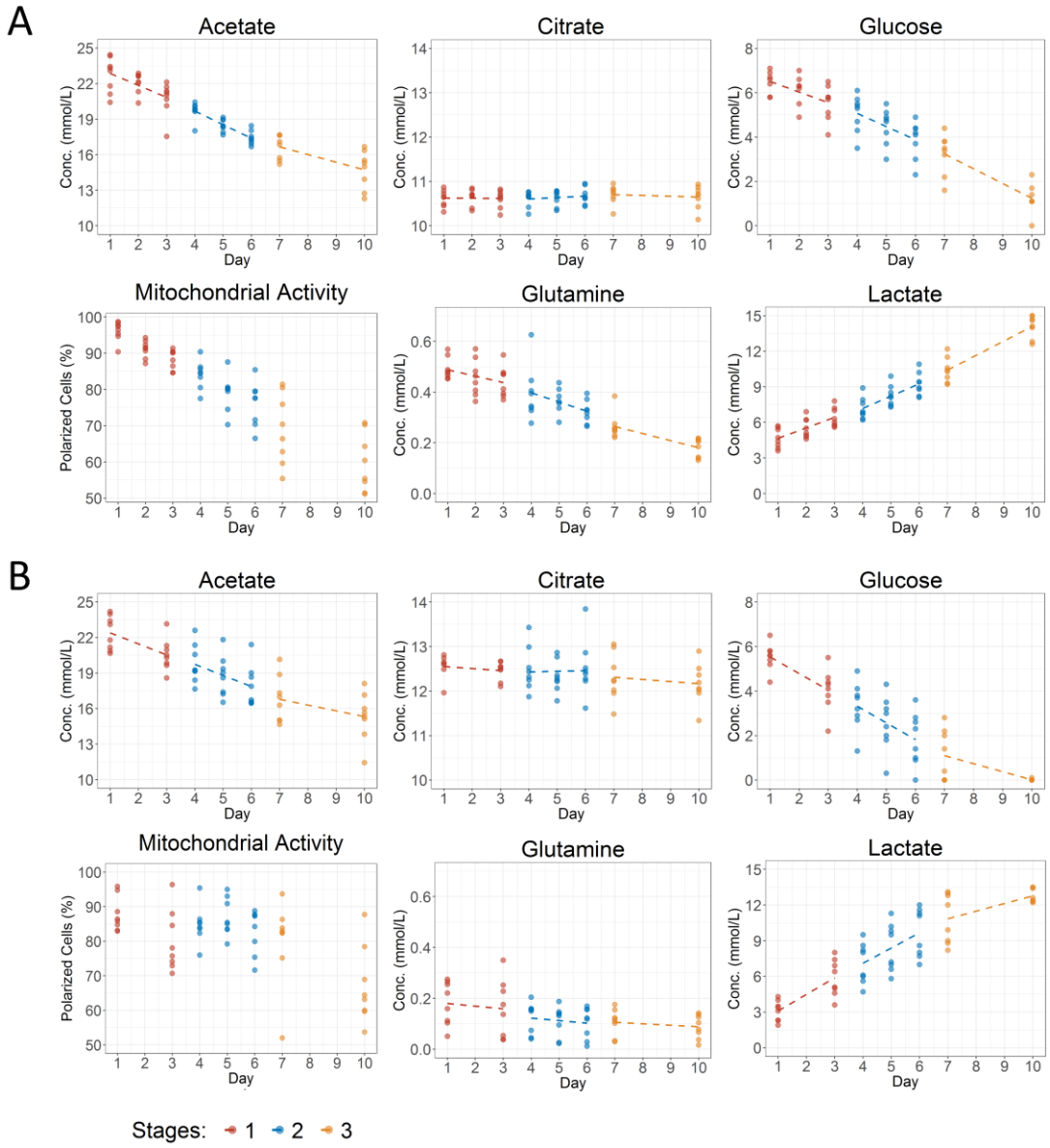

Figure 1. Extracellular concentrations of acetate, citrate, glucose, and glutamine, and percentage of cells with polarized mitochondria at different time points during platelet storage. Eight BC-PCs are shown in panel A and eight AP-PCs in panel B. The storage time is divided into three stages, stage 1 (days 1-3), stage 2 (days 4-6) and stage 3 (days 7-10). For extracellular metabolites, at each stage a line is fit through the measured concentration values. The sign and magnitude of the slopes of the fitted lines define the uptake/secretion rates of the metabolites within iAT-PLT-636.

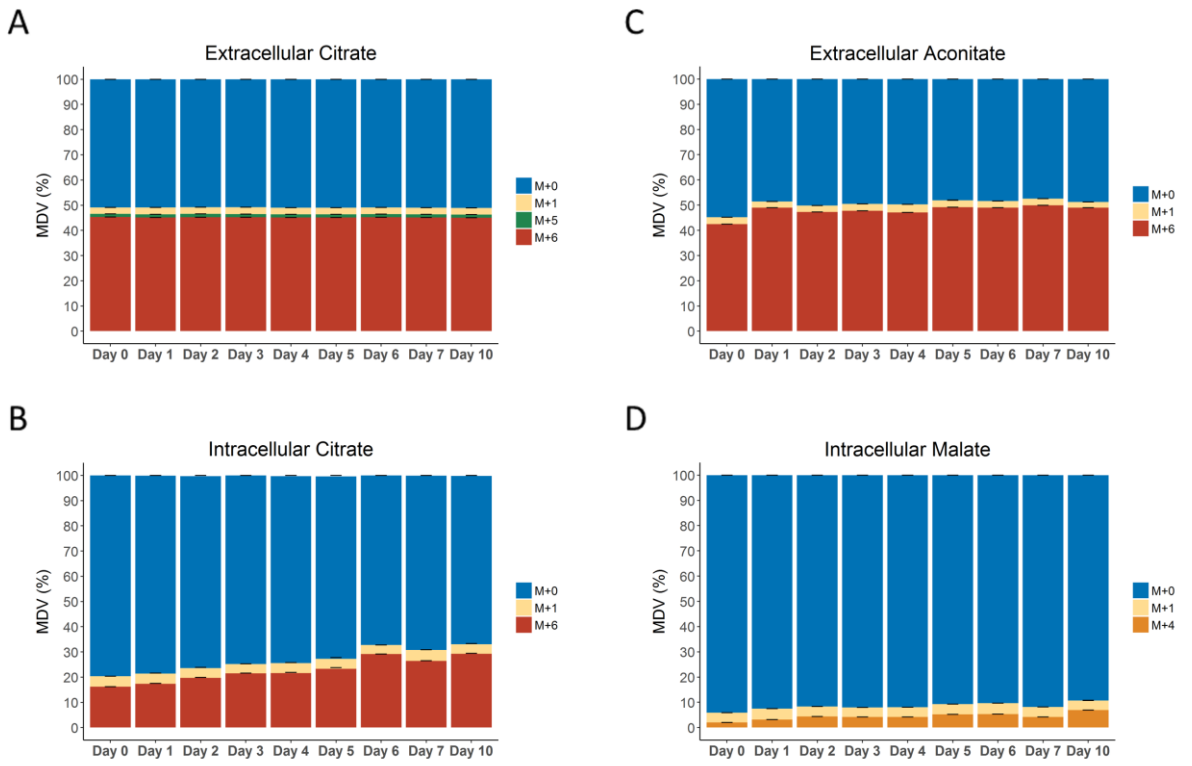

Figure 2. Isotopologue distribution of ^{13}C enriched citrate and malate following addition of UL-^{13}C6 citrate to an AP-PC unit. Label enrichment was detected in 4 metabolites in AP-PC containing uniformly labelled ^{13}C citrate. Except for a small amount of the M+5 in the extracellular citrate, likely due to impurities of the added labeled compound, the only isotopologues detected where the naturally occurring M+0 and M+1, as well as the fully labelled metabolites. **A.** The extracellular citrate label enrichment remained stable during storage with 45.2 % ± 0.1 of the total citrate pool fully labeled. **B.** Intracellular citrate was enriched with 16.2 % ± 0.1 at day 0 on the ^{13}C6 isotopologue, the enrichment of which increased linearly (R2 = 0.87) with time and reached 29.2 % ± 0.1 at day 10. **C.** The extracellular aconitate pool was immediately highly enriched at day 0 of storage with label enrichment comparable to extracellular citrate throughout storage, indicating that the majority of extracellular aconitate originates from extracellular citrate. **D.** Label enrichment was detected in relatively low amounts (< 10 %) in intracellular malate and its relative abundance increases over the storage time. The lack of partially labelled isotopologues indicates that the citrate taken up from the medium is not broken down via the TCA cycle. ***Abbreviations:*** **Mass distribution vector (MDV), isotopologue with n carbon atoms labeled with ^{13}C (M+n).**

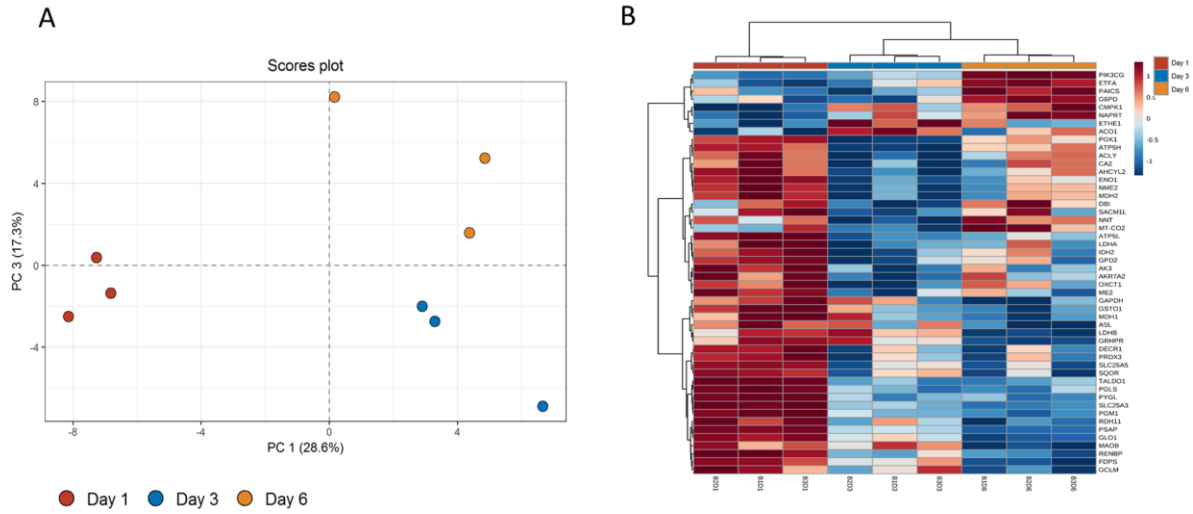

Figure 3. Principal component and hierarchical clustering analysis of metabolic proteins at day 1, 3, and 6 of storage. **A.** Principal component analysis of the metabolic proteins identified by both proteomics methods (n = 160), the numbers in parenthesis represent the total percentage of variance explained by the principal components. The three biological replicates at each time point are represented by the same color. **B.** Hierarchical clustering and a heatmap of the metabolic proteins. Only the 25 proteins contributing the most to the clustering are shown. The majority of the proteins decreases in abundance during the 6 days of storage. The heat map and hierarchical clustering is based on Euclidean distance and Ward‘s method.

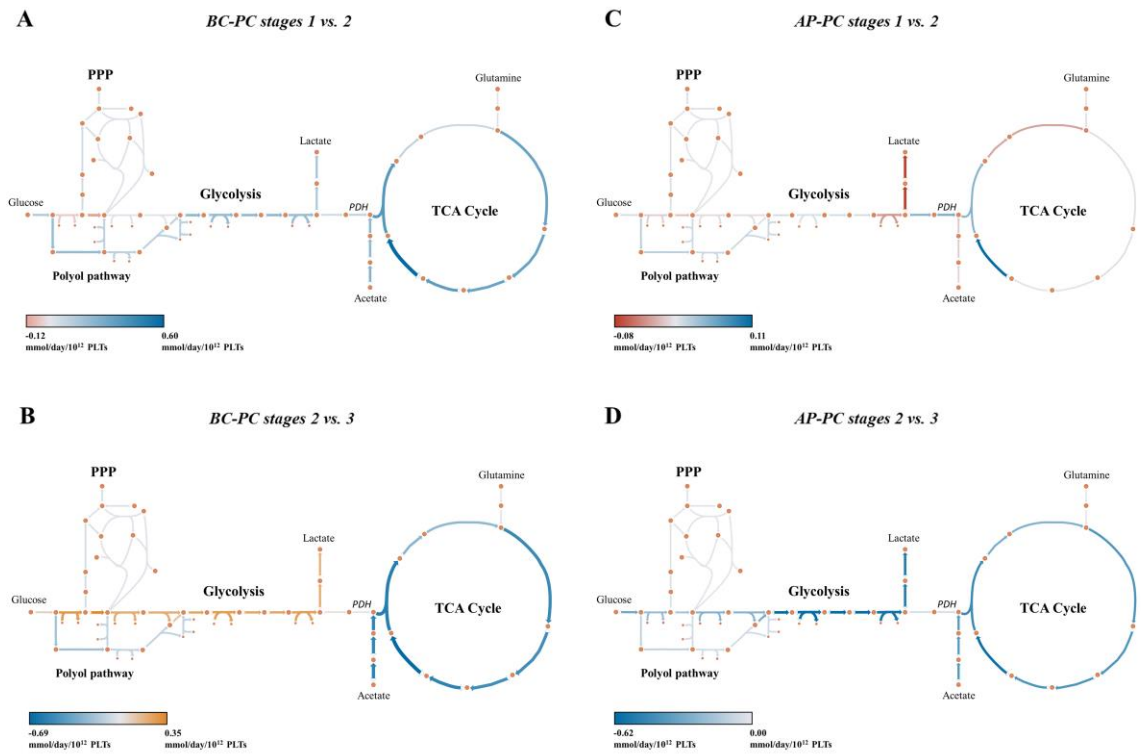

Figure 4. The major energy producing pathways in platelets all have a higher flux during days 4-6 of storage. A schematic overview of predicted flux changes in platelets during storage. The storage time is divided into three stages, stage 1 (days 1-3), stage 2 (days 4-6) and stage 3 (days 7-10). The figure depicts the difference in fluxes in consecutive stages in mmol/day/10^{12} platelets. The flux difference is defined as $V_{kb} - V_{ka}$, with a < b, where V_{kn} is flux through reaction k in mmol/day/10^{12} platelets and b is the stage. Four extracellular metabolites are shown in the figure (glucose, lactate, acetate and glutamine), the flux distribution is however determined by 18-19 extracellular metabolites used to constrain the model (**Table S5**). Metabolites are represented by orange dots and reactions by lines and curves connecting the dots. **A.** Flux changes between the first two stages in BC-PCs, all but two reactions shown have a higher flux value in stage 2 compared to stage 1. The largest difference is found in the reaction of the TCA cycle. **B.** Flux changes between stages 2 and 3 in BC-PCs. During stage 3 there is substantial decrease in acetate consumption and TCA cycle activity, which is compensated with higher flux through glycolysis. **C.** Flux changes between the first two stages in AP-PCs. Flux through energy producing pathways remains relatively stable between stages 1 and 2. Flux through the PDH reaction is predicted to increase substantially, whereas citrate uptake (not shown) decreases. **D.** Flux changes between stages 2 and 3 in AP-PCs. A large decrease in glycolysis in stage 3 is due to glucose depletion in the media. Decrease in mitochondrial energy production at stage 3 is consistent with the results from BC-PC. ***Abbreviations:*** **Pyruvate dehydrogenase (PDH)**